Electrochimica Acta, Vol. 35, No. 9, pp. 1437–1444, 1990.
Printed in Great Britain.

0013–4686/90 $3.00 + 0.00

COMPARATIVE STUDY OF THE PASSIVITY AND THE BREAKDOWN OF PASSIVITY OF POLYCRYSTALLINE IRON IN DIFFERENT ALKALINE SOLUTIONS

O. A. ALBANI,* L. M. GASSA, J. O. ZERBINO, J. R. VILCHE and A. J. ARVIA

Instituto de Investigaciones Fisicoquimicas Teóricas y Aplicadas (INIFTA), Facultad de Ciencias Exactas, Universidad Nacional de La Plata, Suc. 4, C.C. 16, 1900 La Plata, Argentina

(*Received* 30 *October* 1989)

Abstract—The passivity and passivity breakdown of polycrystalline iron is investigated through electrochemical methods complemented with ellipsometry, by employing plain 0.04 M NaOH and saturated $Ca(OH)_2$ solutions with the addition of chloride salt of concentrations up to 1 M. The comparative results indicate that the initial reactions of $Fe(OH)_2$ formation at the inner part of the passive layer level (Fe_3O_4) are only slightly influenced by either the cation or the presence of Cl^- ion in solution, in contrast to their large influence at the outer part of the passive layer (hydrous FeOOH species) where Fe^{2+}/Fe^{3+} redox reactions take place. At high positive potential the breakdown of passivity is also influenced by both Cl^- ion and cation present in solution.

Key words: passivity of iron, passivity breakdown, iron in saturated $Ca(OH)_2$ solutions, ellipsometry of passive iron layers, influence of Cl^- ions on passive iron, composite passive iron layer structure.

1. INTRODUCTION

In alkaline solutions containing chloride ions the values of the breakdown potentials of passive films on iron are rather scattered[1–4] and the mechanism of passivity breakdown particularly regarding the structure and the properties of the surface film is still a matter of discussion. It is agreed that at certain Cl^- ion concentration, pH, and electrode potential values the passivating film is disrupted[5–8]. Recently, *in situ* optical data provided new insights about the chemical composition and structure of the passivity layer electroformed on iron in KOH[9–11], NaOH[12–16], and saturated $Ca(OH)_2$[15–17] solutions.

Raman spectra on iron in 1 M KOH after oxidation–reduction cycles (ORC) at 36 V s^{-1}[9] were interpreted through the formation of Fe_3O_4 although the presence of γ-FeOOH could not be excluded as the very high background of water obscures the spectrum below 300 cm^{-1}. The film formed after ORC at 0.001 V s^{-1} was also assigned to Fe_3O_4[10, 11] although amorphous γ-FeOOH could not be discarded, and that produced after prolonged cycling at 0.05 V s^{-1} was assigned to α-FeOOH grown on top of the passivating layer. These results implied that in the active region iron oxidized to $Fe(OH)_2$ and the latter at higher potentials is further oxidized to α-FeOOH.

On the other hand, ellipsometric measurements of iron in 0.05 M NaOH suggested that a low density FeOOH layer builds up progressively over an inner compact Fe_3O_4 barrier layer after galvanostatic cycling[12], whereas the anodic film produced at different potentials in the passive region after a single potential scan at 80 V s^{-1}[13] was identified as FeOOH for times longer than 2 s, and at shorter times as FeOOH probably containing water.

Ellipsometric results of passive films grown on iron in either saturated $Ca(OH)_2$[17] or 0.05 M NaOH[18] showed no influence of the addition of small amounts of Cl^- ions. In these cases the passive film can be described as that of a complex FeOOH layer whose structure is sensitive to the ionic composition of the solution. Otherwise, potential-modulated reflectance spectra of films formed on iron in 0.1 M NaOH at different high positive potentials by applying an anodic potential sweep at 0.01 V s^{-1}[14] were assigned to magnetite and/or hematite, while in the initial prepassive potential region the presence of Fe(II) in the surface layer was detected. Similar conclusions about the formation of Fe(II) species, probably $FeO \cdot Fe(OH)_2$, in the film potentiostatically produced on iron in 1 M NaOH at relatively high negative potentials arise from X-ray photoelectron spectroscopy data[19] after specimen preparation and transfer in an oxygen-free closed system.

Triangularly modulated triangular potential sweep voltammetry run in the potential region preceding the first anodic current maximum (peak I) in strong alkaline media[7], boric acid–borate buffer solutions[20], and dilute acid and neutral electrolytes containing SO_4^{2-} ions[21], revealed a reversible initial process due to the formation of FeOH species. The subsequent reaction (peak I) generated a thin hydrous $Fe(OH)_2$ layer. Therefore, there are electrochemical[5–8, 20, 22–24], optical[19, 25, 26], and thermodynamic[27] data supporting that the first oxidation level of iron is $Fe(OH)_2$.

This paper is devoted to a comparative study of the influence of Na^+ and Ca^{2+} ions as well as that of Cl^-, in addition to alkaline solutions on the breakdown

*Permanent address: Facultad de Ciencias Exactas Fisicas y Naturales, Universidad Nacional de Misiones, 3300 Posadas, Argentina.

potential (pitting potential) of passivated iron specimens with the aim of establishing protection criteria, particularly for saturated $Ca(OH)_2$ solutions. The latter appears to be a suitable solution to simulate the environment in contact with iron inside pores in concrete media[28–30]. Likewise, new information also emerges by comparing results for the passive film formation on iron in saturated $Ca(OH)_2$ to those obtained earlier for either KOH or NaOH solutions under similar experimental conditions.

2. EXPERIMENTAL

The experimental arrangement was essentially the same as that already described in previous publications[5, 15, 21, 31]. A three-compartment electrolysis Pyrex cell was employed. Polycrystalline iron ("Specpure", Johnson Matthey Chemicals Ltd) working electrodes (specimens) consisted of fixed wires (0.5 mm diameter, 0.25 cm^2 apparent area) and discs (0.85 cm^2 apparent area) in PTFE holders, the borders of the specimen being covered with a small amount of epoxy resin. Each specimen was gradually polished starting with 400 and 600 grade emery papers and finishing with 0.3 and 0.1 μm alumina–acetone suspensions. Afterwards it was cleaned with acetone and repeatedly rinsed with thrice distilled water. Finally, it was cathodically polarized for 5 min in the HER potential region. This treatment furnished an electroreduced specimen with a very reproducible behaviour for the electrochemical measurements. Either an *sce* properly shielded or a hydrogen electrode in the same solution were used through a Luggin–Haber capillary tip as reference electrodes, but potentials in the text are referred to the *nhe* scale. A large-area Pt plate was employed as counter electrode.

The following electrolyte solutions were used: 0.04 M NaOH + x M NaCl and saturated $Ca(OH)_2$ + x M NaCl ($0 \leqslant x \leqslant 1$), pH 12.6. They were prepared from thrice distilled water previously boiled to remove CO_2 and analytical grade (p.a. Merck) reagents. Runs were made at 25°C under purified N_2 gas saturation by applying the following perturbing potentials: (i) conventional triangular potential sweeps either single (STPS) or repetitive (RTPS) between preset cathodic ($E_{s,c}$) and anodic ($E_{s,a}$) switching potentials at different potential sweep rates (v) within the 0.001–0.3 V s^{-1} range; (ii) combined RTPS with STPS; (iii) STPS or RTPS with combined potential steps; (iv) galvanostatic steps at a constant anodic current density, 0.15 mA cm^{-2}, to measure the corresponding pitting potentials.

The electrolysis cell was mounted in a Rudolf Research type 437-02/200 B manual ellipsometer (maximum resolution 0.01°) provided with a 150 W tungsten lamp with filter (546.1 nm) and an RCA 1P 21 photomultiplier. The incidence light beam angle was fixed at 69° and that of the compensator at 135°. Ellipsometric data at fixed wavelength of a freshly polished and electroduced iron electrode at $E = -1.36$ V were initially measured. The corresponding polarizer (P_0) and analyser (A_0) readings yield the refractive index (n_s) and the absorption coefficient (k_s). The complex refractive index, $\bar{n}_s = n_s - ik_s$, derived from P_0 and A_0 is in good agreement with the values for bare iron reported in the literature[32, 33]. The ellipsometric readings (P and A) of the specimen covered with the anodic layer were made at either $E_{s,a}$ or $E_{s,c}$ after applying one of the following perturbing potential programs. The first one (Procedure I) consisted of a potential sweep from -1.36 V upwards at $v = 20$ V s^{-1} followed by a potential holding at different $E_{s,a}$ values to grow and to stabilize the anodic layer during 60 min. Then, ellipsometric readings were made at different times. The second one (Procedure II) implied an RTPS at different v to accumulate an anodic layer at the electrode surface. In any case, the ellipsometric readings are presented as P *vs* A plots ($\delta P = P - P_0$ and $\delta A = A - A_0$).

3. RESULTS AND INTERPRETATION

The STPS and RTPS voltammograms of iron in saturated $Ca(OH)_2$ at $v = 0.1$ V s^{-1} between $E_{s,c} = -1.26$ V and $E_{s,a} = 0.54$ V exhibit four anodic (peak I, II, peak III and III') and four cathodic (VI', peak IV and peak V) contributions (Fig. 1a), as already described in previous publications[5, 15, 16, 34]. The first conjugated pair of peaks I(II)/V is related to the cyclic formation and reduction of the inner part of the passivating layer (ippl). The second conjugated pair of peaks, namely III(III')/IV(IV'), corresponds to the $Fe(II) \rightleftarrows Fe(III) + e^-$ redox reaction occurring at the outer part of the passivating layer (oppl)[15, 16, 34]. The E–j displays depicted in Figs $1b_1$ and $1b_2$ have been recorded through successive STPS with $E_{s,a}$ decreased and increased step-

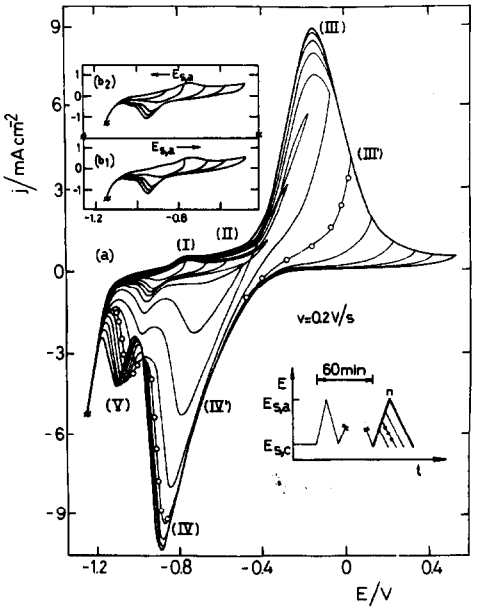

Fig. 1. Influence of the anodic switching potential on the voltammograms of iron run at $v = 0.2$ V s^{-1} in saturated $Ca(OH)_2$. (a) Runs made by changing $E_{s,a}$ downwards after a previous RTPS between -1.26 and 0.54 V to attain the stable voltammogram. (b) Runs made by changing $E_{s,a}$ upwards (b_1) and downwards (b_2) in the potential range of peaks I–II/V after the application of the potential–time program described in Fig. 1a.

wise, respectively. The lower the value of $E_{s,a}$ the greater the depolarization of the electroreduction processes, as peak IV shifts positively. In addition, the charge of peak III up to the peak potential value diminishes, although the value of the peak potential itself remains unaltered. The charges of peaks I and II after baseline correction for peak III become independent of $E_{s,a}$.

Furthermore, for $E_{s,c}$ values sufficiently negative to assure the complete electroreduction of the ippl, the first oxidation level of iron in alkaline solution can be associated with the formation of the $Fe(OH)_2$ monolayer. It should be noted that in the first linear potential sweep run in the positive potential going direction with a fresh polished iron electrode, the contribution of peak III tends to decrease as v increases[31]. It should be noticed that at a constant pH, peak I becomes independent of the electrolyte composition. On the other hand, as $E_{s,a}$ is set at a value more negative than the potential range of peaks III (Figs $1b_1$ and $1b_2$), during the negative going potential excursion peak IV is no longer observed as a single peak, and peak V splits into two contributions.

The anodic layer accumulated after 60 min potential cycling at $v = 0.2\ V\ s^{-1}$ is largely related to the conjugated pair of peaks III/IV, as seen in the dashed voltammogram shown in Fig. 2. However, a different behaviour can be observed by running the voltammogram immediately after cathodizing at $E_{s,c} = -1.26$ V for $\tau = 20$ min. In this case a charge increase in the potential range of the conjugated peaks I(II)/V can be observed. This effect, however, tends to disappear as the potential cycling continues (see full lines in Fig. 2). It is interesting to note that the passive current read at 0.4 V also increases according to the charge of peaks I(II)/V (Fig. 2). The prolonged intermediate cathodization at $E_{s,c}$ favours the formation of Fe(0) in the oxide layer, but the following electrooxidation cycle yielding Fe(II) species does not contribute to the subsequent process related to peak III. Thus, it appears that the accumulation of active Fe(II) species in the oppl proceeds only at the expense of the partial electroreduction of the ippl (barrier layer). Nevertheless, one should not disregard some contribution from the Fe(II) species coming out from Fe(0) electrooxidation to the oppl in the potential range of peak III′. It should be further noted that under comparable experimental conditions iron electrodes in both KOH and NaOH solutions accumulate charge faster and the conjugated peaks III/IV become more reversible than in $Ca(OH)_2$ solutions[15, 16]. Similar conclusions can be derived for the growth of the anodic layer either voltammetrically or potentiostatically, independently of the fact that the thickness of the anodic layer obtained at a constant potential is considerably smaller than that brought about under potential sweeping.

The RTPS voltammogram run in saturated $Ca(OH)_2$ between $E_{s,c} = -1.26$ V and $E_{s,a} = 0.54$ V can be modified by stepping $E_{s,c}$ from -1.26 V to $E'_{s,c}$, a potential value located within the potential range of peaks IV′–IV, for a certain time, τ, and subsequently recording the voltammogram between $E_{s,c}$ and $E_{s,a}$. The comparison of these voltammograms to the initial one (Fig. 3) allows discovery of the differences which can possibly be assigned to ageing effects at the anodic layer. The voltammetric response after the potentiodynamic ageing treatment[7, 34] (Fig. 3a) shows that for values of $E'_{s,c}$ more positive than $E_{p,IV'}$ the intermediate RTPS from $E_{s,a}$ to $E'_{s,c}$ applied during $\tau = 5$ min produces a slight increase in the charge of peaks IV and V, whereas the opposite occurs for the current hump IV′. But as $E'_{s,c}$ is set closer to $E_{p,IV}$ (Fig. 3b), then the contour of peak IV exhibits an ill-defined double peak involving a small charge, and simultaneously the charge of peak V increases considerably. Furthermore, after applying the intermediate RTPS the charge of peak V increases and the corresponding peak potential $E_{p,V}$ shifts negatively as τ increases (not shown here). On the other hand, the rapid decrease in the electroreduction charge of peak IV which is observed for saturated $Ca(OH)_2$ becomes practically cancelled in either KOH or NaOH solutions, although in NaOH

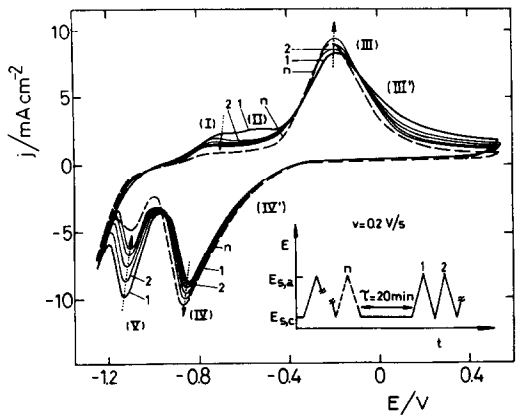

Fig. 2. Voltammogram of iron run in saturated $Ca(OH)_2$ at $v = 0.2\ V\ s^{-1}$ combined with a potential step at $E_{s,c} = -1.26$ V during $\tau = 20$ min after the stable voltammogram (dashed curve) was attained. The arrows indicate the cycling order subsequent to the potential step.

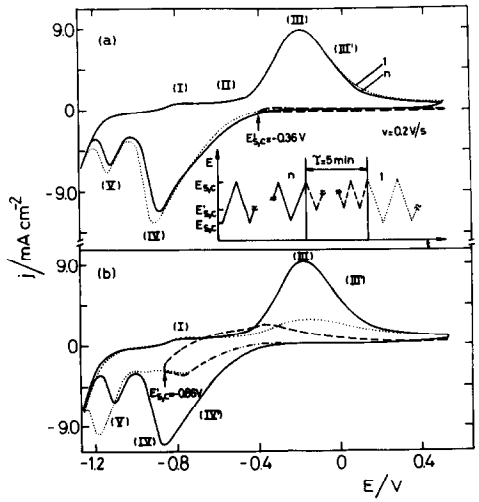

Fig. 3. Voltammograms of iron run at $v = 0.2\ V\ s^{-1}$ in saturated $Ca(OH)_2$. The potential program includes a 60 min RTPS between $E_{s,c} = -1.26$ V and $E_{s,a} = 0.54$ V before applying the intermediate RTPS during $\tau = 5$ min between $E_{s,a}$ and either $E_{s,c} = -0.36$ V (a) or $E_{s,c} = -0.86$ V (b).

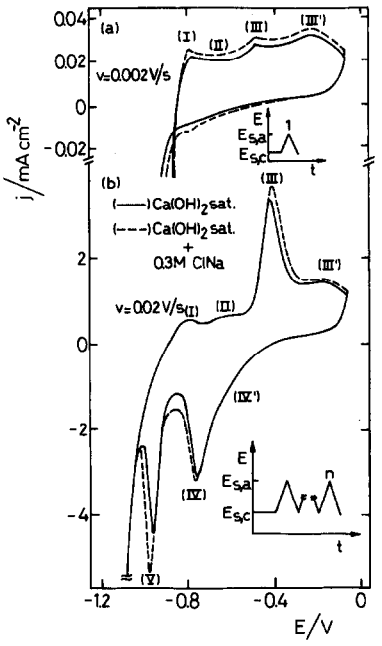

Fig. 4. STPS voltammograms run at $v = 0.002\ V\ s^{-1}$ (a) and RTPS voltammograms run at $v = 0.2\ V\ s^{-1}$ (b); iron in saturated $Ca(OH)_2$ (———); iron in saturated $Ca(OH)_2 + 0.3$ M NaCl (– – –).

solution peak IV splits into two well defined contributions (see, for instance, Fig. 1b in Ref. [7]).

The STPS voltammogram run at $0.002\ V\ s^{-1}$ (Fig. 4a) and the RTPS voltammogram run at $0.02\ V\ s^{-1}$ (Fig. 4b) of iron in saturated $Ca(OH)_2$ (full lines, Fig. 4) are practically unaltered by the addition of NaCl (dashed lines, Fig. 4), at least for NaCl concentrations up to 0.3 M. These voltammograms run between $E_{s,c} = -1.16$ V and $E_{s,a} = -0.06$ V, that is, covering the active to passive transition potential range of iron, suggest that the addition of Cl^- ions has no appreciable influence on the initial formation of the anodic layer.

The pitting potential, E_p, of iron in both 0.04 M NaOH and saturated $Ca(OH)_2$ containing different concentrations of NaCl was measured at $0.15\ mA\ cm^{-2}$ for 300 min. In this case the specimens have been previously cathodized for 5 min at

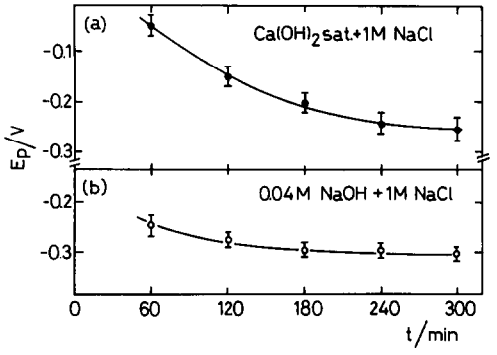

Fig. 5. Anodic galvanostatic potential–time curves resulting at $0.15\ mA\ cm^{-2}$ in saturated $Ca(OH)_2 + 1$ M NaCl (a) and in 0.04 M NaOH + 1 M NaCl (b).

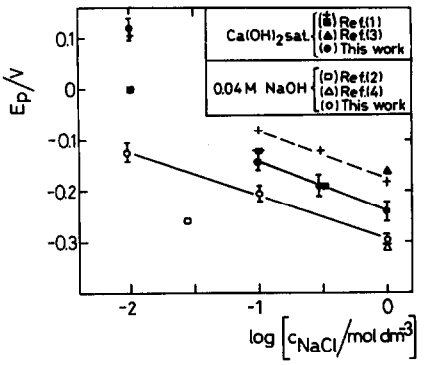

Fig. 6. Comparison of pitting potentials obtained at different concentrations of NaCl in saturated $Ca(OH)_2$ (●) and in 0.04 M NaOH (○) to data reported in the literature.

$0.3\ mA\ cm^{-2}$. The pitting potential–time displays (Fig. 5) are similar for both solutions, but the stationary potential value in saturated $Ca(OH)_2$ (Fig. 5a) is more slowly attained than in 0.04 M NaOH (Fig. 5b). Furthermore, the values of E_p in saturated $Ca(OH)_2$ are slightly more positive than those obtained in NaOH solutions (Fig. 6). This difference increases as the NaCl concentration decreases. For the sake of comparison values of E_p previously reported in the literature have been included in Fig. 6. In general linear E_p *vs* log c_{NaCl} plots can be obtained, their slopes being greater than $-2.303\ RT/F$ ratio. The results shown in Figs 5 and 6 suggest that the anodic layer initially formed on iron in NaOH solutions containing Ca^{2+} ions offers a greater resistance to localized atack by Cl^- ions than that produced in plain NaOH. This difference can also be compared to the voltammetric behaviour of peaks III(III')/(IV')IV in both solutions which are due to the Fe(II)/Fe(III) reaction taking place in the oppl[15].

The ellipsometric data obtained in both electrolytes for anodic products accumulated through either successive potential steps (Procedure I) (Figs 7a and b) or potential cycling (Procedure II) (Figs 8a and b) are rather different. The ellipsometric parameters of the anodic layer resulting from Procedure I show that the initial change in the ellipsometric plots depends mostly on $E_{s,a}$ and to a much lesser extent on the electrolyte composition. For NaOH solution the δP *vs* δA plot (Fig. 7a) exhibits a continuous negative slope, whereas for saturated $Ca(OH)_2$ the opposite slope is observed (Fig. 7b). Nevertheless, the common first change observed in the δP *vs* δA plots when the potential $E_{s,a}$ is applied can be attributed to the initial formation of the ippl. The optical parameters of the ippl can be described through a single layer model[35] by taking $n = 2.2$ and $k = 0.4$ (Fig. 7c).

On the other hand, the ellipsometric data resulting from Procedure II at $0.2\ V\ s^{-1}$ and -1.26 V change gradually in going from the 1st to the 3rd potential scan. The direction and magnitude of these changes, which depend on the electrolyte composition (Figs 8a and b), can seemingly be compared to those derived from Figs 7a and b after 60 min anodization at $E_{s,a}$. Then, the ellipsometric changes indicate that an oppl of similar characteristics has been grown either under anodic polarization or under potential cycling. Nevertheless, the accumulation of surface products in

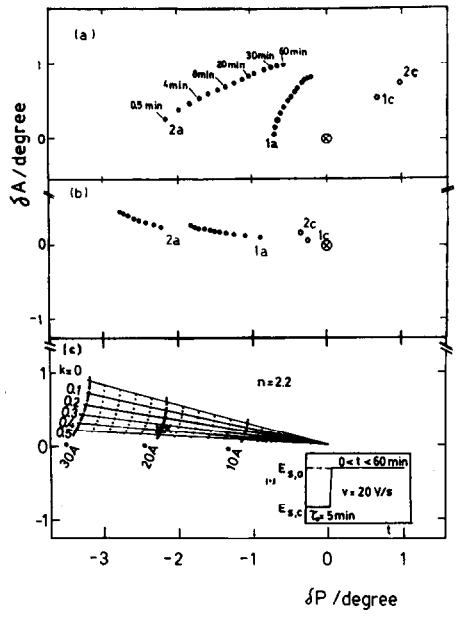

Fig. 7. Ellipsometric plots obtained at $E_{s,c} = -1.26$ V (open symbols, 1c and 2c) and at $E_{s,a} = -0.44$ V (full points, 1a) and $E_{s,a} = 0.12$ V (full points, 2a). The program involves a potential scan at $v = 20\ V\ s^{-1}$ from $E_{s,c}$ to $E_{s,a}$ followed by a potential step at $E_{s,a}$ during 60 min. (a) Saturated $Ca(OH)_2$; (b) 0.04 M NaOH. (c) Theoretical plots computed for $n = 2.2$ and different k and film thickness values on the basis of the single layer model[35]. Experimental data (×) measured at −0.44 and 0.12 V in both electrolyte solutions immediately after the potential scan at $v = 20\ V\ s^{-1}$ from $E_{s,c} = 1.26$ V up to $E_{s,a}$. The symbol (⊗) corresponds to the electroreduced iron electrode after potential holding for 10 min at $E_{s,c}$.

the oppl through potential cycling occurs at the expense of the oxidation–reduction cycles involving the ippl, as can be seen through the changes of P and A brought about at high negative potentials (Figs 8a and b).

As the global optical parameters involve both the ippl and the oppl, the changes of δP and δA exclusively related to the oppl can be estimated provided that a correction for the presence of the ippl can be made (Fig. 7c). The reduced state of the oppl constitutes the surface layer on iron at high negative potentials, whereas at high positive potentials the changes in the δP *vs* δA plot can be related to the variation of the optical parameters for the oppl, as the characteristics of the ippl formed at a constant $E_{s,a}$ are independent of potential cycling. Under these conditions, the single film model can be extended to a model involving two superposed different homogeneous oxide layers[35]. The theoretical ellipsometric data obtained for the oppl layer in saturated $Ca(OH)_2$ are consistent for values of $n \geqslant 1.332$ (Fig. 8a′) and in 0.04 M NaOH for $n \approx 1.44$ (Fig. 8b′), respectively, and a low value of k in both cases, $k \approx 0.005$. The theoretical δP *vs* δA plots shown in Figs 8a′ and b′ suggest that the changes of the ellipsometric data can be interpreted as the contribution of two single film models, one corresponding to the ippl (dotted curves), and the other one to the oxidized state of the oppl at $E_{s,a}$ (dashed curves). The comparison of the electrochemical and the ellipsometric data in saturated $Ca(OH)_2$ and in NaOH solutions at the same pH shows that the characteristics of the ippl become independent of the electrolyte, whereas the properties of the oppl which apparently behaves as a gel-like iron hydroxide structure depend on the cation in solution. It should be noted that the ippl has been identified as Fe_3O_4[15]. In saturated $Ca(OH)_2$ the values of P and A for the oppl are consistent with a practically constant layer thickness of about 2100 Å and a value of $n \geqslant 1.332$ which gradually increases during cycling (Fig. 8a′). Otherwise, in NaOH solution the thickness of the oppl increases continuously with a constant n value (Fig. 8b′). The differences in the behaviour of iron in $Ca(OH)_2$ and NaOH appear also through the ellipsometric readings at $E_{s,c}$ where the metal is covered by the reduced outer layer. It should be noted that the Fe(II)/Fe(III) redox process taking place in the oppl during the oxidation–reduction cycles has also been observed at precipitated hydrous iron hydroxide layers chemically formed on inert conducting substrates[34, 36, 37].

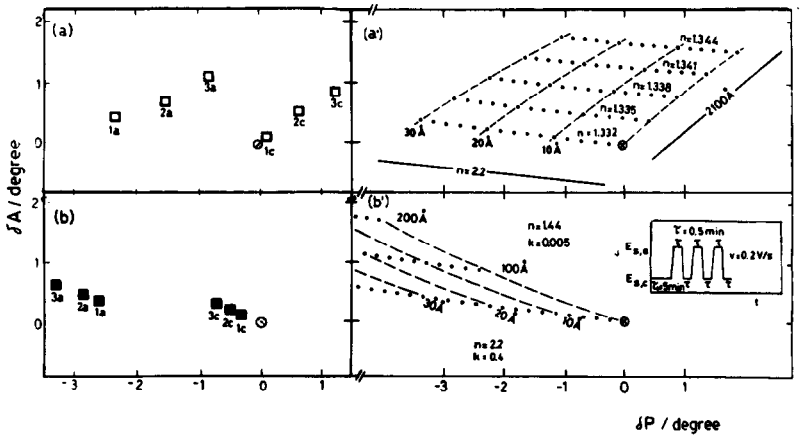

Fig. 8. Ellipsometric plots for the anodic layer formed at $E_{s,a} = 0.1$ V (symbols 1a, 2a and 3a) and at $E_{s,c} = -1.26$ V (symbols 1c, 2c and 3c) from the 1st, 2nd and 3rd potential scans at $0.2\ V\ s^{-1}$. (a) Saturated $Ca(OH)_2$; (b) 0.04 M NaOH. Theoretical plots for saturated $Ca(OH)_2$ (a′) and 0.04 M NaOH (b′) at $E_{s,a}$ and $E_{s,c}$.

4. DISCUSSION

As far as the influence of Ca^{2+}, Na^+, and Cl^- ions on the passivity and passivity breakdown of iron in alkaline solutions is concerned, the preceding analysis of results provides a reasonable amount of information which can be discussed in terms of the initial reaction, that is, the early stages of the ippl formation, the influence of Cl^- ions in the Fe^{2+}/Fe^{3+} reaction at the oppl, the participation of Ca^{2+} ions at the level of the oppl and, finally, the influence of those anions and cations in the breakdown of passivity.

4.1. *The early stages of the ippl formation*

Voltammetric results show that the electrooxidation of the base metal surface of $Fe(OH)_2$ in the potential region of peak I (Figs 1–4) is in agreement with the data obtained in other electrolytes in the 6.5–14 pH range[5, 20]. This similarity extends to the location, charge density, and contour of peak I. Therefore, the reaction yielding the first monolayers of $Fe(OH)_2$ on the base metal depends on the alkaline solution but it becomes independent of the cation, and also practically unaffected by the presence of Cl^- ions (Fig. 4). Furthermore, the accumulation of Fe_3O_4 takes place at potentials higher than that of peak I and it occurs during each positive potential going scan. Otherwise, after a prolonged cathodization at $E_{s,c}$ (Fig. 2) the hydrous iron hydroxide surface layer undergoes a partial electroreduction to Fe(0). This fact produces an increase of the voltammetric charge associated with peak I during the following voltammetric cycles due to the contribution of the anodic oxidation of Fe(0) resulting from the preceding surface layer electroreduction.

In alkaline solution the high adsorbability of OH^- ions determines that the first step of the corrosion and passivation reaction of iron, that is, the reaction:

$$Fe + OH^- = Fe(OH^-)_{ad} = FeOH_{ad} + e^-, \quad (1)$$

be scarcely influenced by the presence of a low concentration of Cl^- ions. Nevertheless, as the latter increases, competitive adsorption processes such as:

$$Fe(OH^-)_{ad} + Cl^- = Fe(Cl^-)_{ad} + OH^-, \quad (2)$$

and:

$$Fe(OH)_{ad} + Cl^- = Fe(Cl)_{ad} + OH^-, \quad (3)$$

become increasingly important. In these cases, the anodic dissolution of Fe as a complete anionic species impedes the formation of the passivating oxide layer on iron. This type of process has been extensively considered, mostly in relation to the corrosion of iron family metals in acid solutions (see Ref. [38] and references therein).

4.2. *The influence of* Cl^- *ions at the composite passive layer level*

In the potential range of peak II the prepassive $Fe(OH)_2$ layer is converted to a composite Fe_3O_4 barrier layer whose thickness increases in the passive region according to the electrode potential (Fig. 1). Recent electrochemical and ellipsometric transients run at a constant potential for iron in 0.04 M NaOH[31] revealed that the variation of both the optical parameters and the current with time depended on the incorporation of NaCl up to 0.05 M even after a previous prolonged anodization in the plain base solution. These variations operated in the direction of decreasing refractive index of the passivating film probably due to slight decrease in thickness (< 10%) of the ippl or to defects induced in the oxide structure[16]. Recent measurements[39] employing radiotracer techniques indicated adsorption and absorption of Cl^- ions on passive iron in borate buffer, with time constant values of about 1 and 60 min, respectively. It is clear that at potentials more positive than the potential of peak III, the presence of Cl^- ion favours the rupture of the passivating layer (Figs 5 and 6).

The values of the pitting potential decrease as the NaCl increases approaching within the error of the measurements a linear E_p *vs* $\log c_{NaCl}$ relationship with a slope close to $-2.303\,RT/F$. This is the type of dependence which should be expected for an increasing influence of the aggressive anion. Nevertheless, at a constant Cl^- ion concentration the influence of the latter on the E_p value in $CaCl_2$ solution is milder than in NaOH solution. In this respect it is clear that at potentials exceeding the E_p value, Cl^- ions assist the disrupture of the passivating layer, that is the ippl suffers equally the attack both in NaOH and $Ca(OH)_2$ solutions[16].

On the other hand, the redox characteristics of the oppl are not considerably modified due to the presence of Cl^- ions, except that the voltammetric charge is increased because of the attack of the base metal in the alkaline solution, accumulating further amounts of FeOOH species.

4.3. *Specific influence of* Ca^{2+} *ions as compared to* Na^+ *ions*

The influence of Ca^{2+} ions on the electrochemical and ellipsometric response of iron in alkaline solution reflects particularly at the oppl level. This means that the effect of Ca^{2+} ions should be related to changes in the structure of the FeOOH part of the passivating layer. It is known that α-FeOOH is an oxygen deficient oxide which has a crystal structure close to that of α-Fe_2O_3[40]. The low electronic conductivity of α-FeOOH is explained by the hopping of *d* electrons on Fe(II) to Fe(III)[41]. For this type of oxygen deficient oxides the occupancy of a foreign metal ion produces an enhancement of either the *n*-type or the *p*-type semiconductor behaviour, depending whether the valency of the incorporated cation is larger or lower, respectively, of that of the normal cation site. In the case of α-FeOOH this type of effect has been investigated by adding either tetravalent cations such as Ti^{4+}, Ge^{4+} and Sn^{4+}, or divalent cations such as Ca^{2+}, Mg^{2+} and Cu^{2+}[41]. The addition of Cu(II), for instance, favours an amorphous state. Accordingly, it is possible that the nature of the cation in solution changes the properties of the oppl. Thus, in $Ca(OH)_2$ solution the local coprecipitation of Ca^{2+} can include the $Fe(OH)_2$ and FeOOH species in the composite passivating layer, where the FeOOH species presumably behaves as a valence controlled α-FeOOH structure where the electrical conductivity is modified through a mechanism similar to that of valence control in hydroxides with defect chemical reactions[42], so that

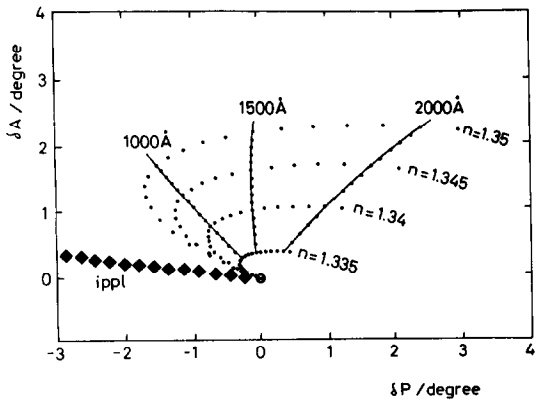

Fig. 9. Ellipsometric plots computed for $k = 0$, thicknesses in the $0 < d \leqslant 2100$ Å range and $n = 1.335$, 1.34, 1345, and 1.35 values, on the basis of the single layer model[35]. Full symbols (◆) correspond to the ippl for $n = 2.2$ and $k = 0.4$.

the change in the electrical conductivity is mainly due to the carrier concentration rather than the change in mobility. This explanation appears to be consistent with the n and k values for the oxidized and reduced passivating layer observed for NaOH and saturated $Ca(OH)_2$ solutions. The reduced state of the thin surface layers formed in NaOH could be related to a film with $n = 1.44$ and $0.005 \leqslant k \leqslant 0.010$ for thickness continuously increasing up to about 1400 Å. Otherwise, the ellipsometric results obtained for the oppl formed in $Ca(OH)_2$ solution (Fig. 9) can be explained through the optical indices $1.332 < n < 1.35$ and $k \geqslant 0$. At constant n, the increase of k corresponds to an increase in the calculated value of δA[15]. The calculated ellipsometric plot shows that in the $0° \leqslant \delta P \leqslant 2°$ and $0° \leqslant \delta A \leqslant 2°$ ranges, values of n smaller than 1.35 are required to account for the experimental data. Such low values of n are associated with a low density oxide layer. For such a situation it is possible to interpret the ellipsometric behaviour of the oppl during potential cycling through a constant thickness film ($\approx$2100 Å) with n increasing from a value close to that of the solution to $n \approx 1.35$. This explanation is consistent with a precipitation process in a saturated metal hydroxide solution.

To estimate the amount of iron hydroxide in the oppl, let us consider the change of δA corresponding to a constant surface layer involving a composite iron hydroxide–electrolyte solution structure. The theories for the dielectric constant of a composite layer predict linear dependences of n and k on the volume fraction of their constituents[43]. Accordingly, for the same amount of anodic product different thicknesses of the surface layer contain different volume fractions of iron hydroxide. Under these circumstances, for two effective optical indices n_1 and n_2, and k_1 and k_2, the corresponding surface layer thicknesses, d_1 and d_2, satisfy the equations:

$$(n_1 - n_0)d_1 = (n_2 - n_0)d_2, \tag{4}$$

and:

$$k_1 d_1 = k_2 d_2, \tag{5}$$

where n_0 is the refractive index of the electrolyte solution, $n_0 = 1.332$. In order to evaluate the change of the oppl ellipsometric parameters observed in saturated $Ca(OH)_2$ the following indices have been chosen: $n_1 = 1.44$ and $k_1 = 0.005$. It is noteworthy that these values correspond to an oppl relatively more compact than that formed in NaOH solution.

The values of n_2 and k_2 corresponding to the relatively less compact oppl formed in $Ca(OH)_2$ solution for $d_2 \leqslant 2100$ Å can be expressed as:

$$n_2 = n_0 + \alpha(n_1 - n_0), \tag{6}$$

and:

$$k_2 = \alpha k_1, \tag{7}$$

where α denotes the apparent volume fraction of the iron hydroxide in the composite layer, which varies between 0 for $n_2 = n_0 = 1.332$ (pure electrolyte) and 1 for $n_2 = n_1$ (compact oppl formed in NaOH solution). Equations (4)–(7) allow us to correlate the optical parameters n_2 and k_2 for different d_2 values, as seen in Fig. 10.

The changes of the δP *vs* δA plot observed during the first three potential cycles are larger for iron in $Ca(OH)_2$ solution than those obtained in NaOH solution. This effect can be associated with an amount of iron precipitated in $Ca(OH)_2$ solution which is greater than that formed in NaOH solution, although the oppl formed in NaOH solutions appears to be more compact than that produced in $Ca(OH)_2$ solution.

The influence of the cations in the characteristics of the passivation layer can also be related to the differences in their hydration energies and charge/size ratio as well as to the stronger adsorption of Ca^{2+} ions as compared to Na^+ ions at the outer plane of the ippl. These effects should favour the presence of Ca^{2+} ions at the oppl. On the other hand, the greater apparent volume fraction of electrolyte at the oppl

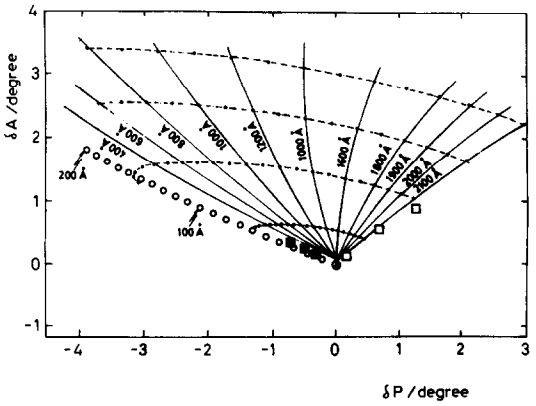

Fig. 10. Ellipsometric plot calculated on the basis of the single layer model[35]. Open symbols (○) correspond to the most compact (limiting case) oppl with constant volume fraction of iron hydroxide for $n = 1.44$ and $k = 0.005$. Full points correspond to a constant thickness less compact oppl (dashed curves) and at to a layer with a constant volume fraction of iron hydroxide (full curves) as described by equations (4)–(7) in the text. Experimental results obtained at $E_{s,c} = -1.26$ V in NaOH (■) and in saturated $Ca(OH)_2$ (□) solutions during the first three potential cycles according to Procedure II are included.

produced in $Ca(OH)_2$ solution probably contributes to make the local acidification effect occurring during the breakdown of the ippl smoother.

The fact that at a constant Cl^- ion concentration, the value of E_p in saturated $Ca(OH)_2$ becomes more positive than in 0.04 M NaOH, indicates a greater protection promoted by the presence of Ca^{2+} at the oppl which derives from the specific characteristics imposed by the cation to the passivating layer. This fact can be used to envisage new protection criteria of metals in aggressive media.

In the presence of corrosion activators $Ca(OH)_2$ plays an important role as inhibitor for carbon steel[44]. However, for the practical case of steel in concrete, it is rather difficult to attempt to define either a threshold chloride content or a critical c_{Cl^-}/c_{OH^-} ratio as a corrosion protection criterion because other factors such as the steel to mortar adhesion, the formation of voids at the steel/mortar interface, the oxygen and water contents, and the anode to cathode area ratio, also have a considerable influence on the corrosion process[45, 46].

Acknowledgements—This work was supported by the Consejo Nacional de Investigaciones Cientificas y Técnicas and the Comisión de Investigaciones Cientificas de la Provincia de Buenos Aires.

REFERENCES

1. J. F. Henriksen, *Corros. Sci.* **20,** 1241 (1980).
2. V. K. Gouda, *Br. Corros. J.* **5,** 198 (1970).
3. W. J. Tomlinson and M. Wedgeburg, *Surf. Coat. Technol.* **29,** 357 (1986).
4. M. G. Alvarez and J. R. Galvele, *Corros. Sci.* **24,** 27 (1984).
5. R. S. Schrebler Guzmán, J. R. Vilche and A. J. Arvia, *Electrochim. Acta* **24,** 395 (1979).
6. G. Nazri, E. Yeager and B. D. Cahan, Tech. Rep. No. 1, Proj. NR SRO-009/7-30-79, Case Western Reserve University, Cleveland (1981).
7. R. S. Schrebler Guzmán, J. R. Vilche and A. J. Arvia, *J. appl. Electrochem.* **11,** 551 (1981).
8. K. E. Heusler, in *Encyclopedia of Electrochemistry of the Elements* (Edited by A. J. Bard), Vol. 9A, pp. 229–381, Marcel Dekker, New York (1982).
9. M. Froelicher, A. Hugot-Le Goff, C. Pallota, R. Dupeyrat and M. Mason, in *Passivity of Metals and Semiconductors* (Edited by M. Froment), pp. 101–105, Elsevier, Amsterdam (1983).
10. J. Dunnwald, R. Losy and A. Otto, in *Passivity of Metals and Semiconductors* (Edited by M. Froment), pp. 107–112, Elsevier, Amsterdam (1983).
11. J. Dunnwald and A. Otto, *Z. Anal. Chem.* **319,** 738 (1984).
12. Z. Q. Huang and J. L. Ord, *J. electrochem. Soc.* **132,** 24 (1985).
13. T. Zakroczymski, C. J. Fan and Z. Sklarska-Smialowska, *J. electrochem. Soc.* **132,** 2862 (1985).
14. C. Gutiérrez and M. A. Martinez, *J. electrochem. Soc.* **133,** 1873 (1986).
15. O. A. Albani, J. O. Zerbino, J. R. Vilche and A. J. Arvia, *Electrochim. Acta* **11,** 1403 (1986).
16. S. Juanto, J. O. Zerbino, J. R. Vilche and A. J. Arvia, in *Surfaces, Inhibition and Passivation* (Edited by E. McCafferty and R. J. Brodd), pp. 226–238, The Electrochemical Society, Pennington, NJ (1986).
17. H. Oranowska and Z. Szklarska-Smialowska, *Corros. Sci.* **21,** 735 (1981).
18. T. Zakroczymski, C. J. Fan and Z. Sklarska-Smialowska, *J. electrochem. Soc.* **132,** 2868 (1985).
19. S. Haupt, C. Calinski, U. Collisi, H. W. Hoppe, H. D. Speckmann and H. H. Strehblow, *Surf. Interf. Anal.* **9,** 357 (1986).
20. M. E. Vela, J. R. Vilche and A. J. Arvia, *J. appl. Electrochem.* **16,** 490 (1986).
21. J. O. Zerbino, J. R. Vilche and A. J. Arvia, *J. appl. Electrochem.* **11,** 703 (1981).
22. D. S. Poa, J. F. Miller and N. P. Yao, 164th Meeting of the Electrochemical Society, Ext. Abstr. No. 11. (1983).
23. A. Wieckowski and E. Ghali, *Electrochim. Acta* **30,** 1423 (1985).
24. V. S. Muralidharan and M. Veerashanmugamani, *J. appl. Electrochem.* **15,** 675 (1985).
25. J. O'M. Bockris, M. A. Genshaw and V. Brusic, *Symp. Faraday Soc.* **4,** 177 (1970).
26. M. Froelicher, A. Hugot-Le Goff and V. Jovanicevic, in *Passivity of Metals and Semiconductors* (Edited by M. Froment), pp. 85–88, 491–495, Elsevier, Amsterdam (1983).
27. R. Nishimura and N. Sato, Proceedings of the 9th International Congress on Metal Corrosion (ICMC, Jul. 1984, Toronto), Vol 1, pp. 96–101, National Research Council of Canada, Ottawa (1984).
28. D. A. Hausmann, *Mater. Prot.* **11,** 19 (1967).
29. H. Viefhaus and M. Janik-Czachor, *Werkstoffe Korros.* **28,** 219 (1977).
30. C. M. Hansson and J. B. Markussen, *Cement and Concr. Res.* **15,** 65 (1985).
31. S. Juanto, J. O. Zerbino, M. I. Miguez, J. R. Vilche and A. J. Arvia, *Electrochim. Acta* **32,** 1743 (1987).
32. N. Sato and K. Kudo, *Electrochim. Acta* **16,** 447 (1971).
33. N. Sato, *Boshoku Gijutsu* **23,** 535 (1974).
34. J. R. Vilche and A. J. Arvia, *Acta Cient. Venezolana* **31,** 408 (1980).
35. F. L. McCracking, Mat. Bur. Stand. Tech. Note 479, U.S. Govt. Printing Office, Washington (1969).
36. V. A. Macagno, J. R. Vilche and A. J. Arvia, *J. appl. Electrochem.* **11,** 417 (1981).
37. M. C. Galindo, M. E. Martins, J. R. Vilche and A. J. Arvia, *J. appl. Electrochem.* **20,** 102 (1990).
38. S. G. Real, J. R. Vilche and A. J. Arvia, *Corros. Sci.* **20,** 563 (1980).
39. V. Jovanicicevic, J. O'M. Bockris, J. L. Carbajal, P. Zelenay and T. Mizuno, *J. electrochem. Soc.* **133,** 2219 (1986).
40. K. Kaneko, M. Serizawa, T. Ishikawa and K. Inouye, *Bull. Chem. Soc. Jpn* **48,** 1764 (1975).
41. K. Kaneko and K. Inouye, *Bull. Chem. Soc. Jpn* **47,** 1139 (1974); *ibid.* **49,** 3689 (1974); *ibid.* **52,** 315 (1979).
42. K. Kaneko, N. Inoue and T. Ishikawa, *J. phys. Chem.* **93,** 1988 (1989).
43. D. E. Aspnes, *Handbook of Optical Constants of Solids,* Ch. 5, p. 89, Academic Press, New York (1985).
44. A. P. Akol'zin, P. Ghosh and Yu. Ya. Kharitonov, *J. electrochem. Soc. India* **33,** 177 (1984); *Br. Corros. J.* **20,** 1 (1985).
45. R. F. Stratfull, *Corrosion* **43,** 483 (1987).
46. T. Yonezawa, V. Ashworth and R. P. M. Procter, *Corrosion* **44,** 489 (1988).